Cardiovascular Research (2014) **104**, 489–500
doi:10.1093/cvr/cvu227

Aggravation of cardiac myofibroblast arrhythmogeneicity by mechanical stress

Teddy Grand†, Nicolò Salvarani†, Florian Jousset, and Stephan Rohr*

Department of Physiology, University of Bern, Bühlplatz 5, CH-3012 Bern, Switzerland

Received 7 April 2014; revised 15 September 2014; accepted 5 October 2014; online publish-ahead-of-print 24 October 2014

Time for primary review: 38 days

Aims Myofibroblasts (MFBs) as appearing in the myocardium during fibrotic remodelling induce slow conduction following heterocellular gap junctional coupling with cardiomyocytes (CMCs) in bioengineered tissue preparations kept under isometric conditions. In this study, we investigated the hypothesis that strain as developed during diastolic filling of the heart chambers may modulate MFB-dependent slow conduction.

Methods and results Effects of defined levels of strain on single-cell electrophysiology (patch clamp) and impulse conduction in patterned growth cell strands (optical mapping) were investigated in neonatal rat ventricular cell cultures (Wistar) grown on flexible substrates. While 10.5% strain only minimally affected conduction times in control CMC strands (+3.2%, n.s.), it caused a significant slowing of conduction in the fibrosis model consisting of CMC strands coated with MFBs (conduction times +26.3%). Increased sensitivity to strain of the fibrosis model was due to activation of mechanosensitive channels (MSCs) in both CMCs and MFBs that aggravated the MFB-dependent baseline depolarization of CMCs. As found in non-strained preparations, baseline depolarization of CMCs was partly due to the presence of constitutively active MSCs in coupled MFBs. Constitutive activity of MSCs was not dependent on the contractile state of MFBs, because neither stimulation (thrombin) nor suppression (blebbistatin) thereof significantly affected conduction velocities in the non-strained fibrosis model.

Conclusions The findings demonstrate that both constitutive and strain-induced activity of MSCs in MFBs significantly enhance their depolarizing effect on electrotonically coupled CMCs. Ensuing aggravation of slow conduction may contribute to the precipitation of strain-related arrhythmias in fibrotically remodelled hearts.

Keywords Arrhythmia • Slow conduction • Fibrosis • Myofibroblast • Strain

1. Introduction

Old age, genetic predisposition, and insults to the heart like mechanical overload and infarction are well-established causes of fibrotic remodelling of the working myocardium.[1] Remodelled tissue is characterized by the presence of excess amounts of collagen that compromises mechanical pump function and promotes arrhythmogenesis by disruption of the normally uniform electrical substrate for impulse propagation.[2] Excess secretion of extracellular matrix proteins is primarily attributed to 'activated' fibroblasts (myofibroblasts, MFBs) that appear in the working myocardium of diseased hearts.[3] Apart from contributing to structural tissue remodelling, MFBs have been shown to exert direct arrhythmogenic effects on cardiomyocytes (CMCs) following the establishment of heterocellular gap junctional coupling based on connexin 43 (Cx43) and connexin 45 (Cx45) in cell culture systems.[4] In the presence of heterocellular gap junctional coupling, experiments showed that depolarizing current flow from moderately polarized MFBs to well-polarized CMCs causes the latter to undergo partial depolarization thereby inducing slow conduction, precipitation of ectopic activity, and initiation of re-entrant arrhythmias.[5–7]

In contrast to cell cultures grown on rigid substrates that undergo isometric contractions, intact cardiac tissue exhibits phasic length changes during the pump cycle with maximal strain present in end-diastole. With few exceptions, it has generally been found that stretching healthy cardiac tissue within physiological limits (from slack length to the length of maximal tension development) causes a proportional increase in conduction velocities (θ) when measured in observer coordinates (θ_{observ} as obtained, e.g. from optical recordings), while conduction

* Corresponding author. Tel: +41 31 631 87 46; fax: +41 31 631 46 11, Email: rohr@pyl.unibe.ch

† T.G. and N.S. contributed equally to this study.

times between two specific reference points within the stretched tissue (CT_{prep}) remain largely unchanged (for detailed review cf.[8]). While these findings are normally discussed in the framework of CMC stretch sensitivity, work by Kamkin *et al.* suggested that cardiac fibroblasts may be involved in the response of the myocardium to stretch as well. They reported that mechanical stress causes changes in fibroblast polarization due to activation of mechanosensitive channels (MSCs) that may, if electrotonically coupled to CMCs, affect the electrophysiology of the latter.[9] Similarly, Kohl *et al.* have shown in a model that strain-induced fibroblast depolarization may affect the discharge rate of electrotonically coupled sinoatrial pacemaker cells, thereby contributing to the adaptation of the heart rate to atrial filling pressure.[10]

Given these findings, the question arises to which extent MFBs may modulate conduction velocities in diseased fibrotic myocardia subjected to stretch and relaxation. Because a direct investigation of this question in intact tissue exhibiting a complex cellular composition and architecture is not feasible with presently available methodologies, we developed an *in vitro* cell culture system with controlled geometry and defined cellular composition that permits the direct assessment of the differential contribution of CMCs and MFBs to changes of θ during application of defined levels of stretch and relaxation. Using this model, we investigated the hypotheses that (i) immunocytochemically defined cardiac MFBs respond to stretch with a reduction in membrane polarization, that (ii) stretch-induced depolarization of MFBs aggravates slow conduction in strands of electrotonically coupled CMCs, and that (iii) mechanical strain exerted by contractile MFBs on adjacent CMCs may directly affect propagation. Our findings show that physiological levels of longitudinal fibre strain as observed in intact healthy tissue during diastolic filling ($<10\%$)[11] have no significant effects on CT_{prep} in preparations consisting predominantly of CMCs. In the presence of electrotonically coupled MFBs, however, CT_{prep} increases proportionally to applied stretch, suggesting that MFBs act as potent sensors of mechanical stress that cause substantial slowing of conduction in electrotonically coupled CMCs. Such MFB-mediated sensitization of fibrotic cardiac tissue to strain may contribute to the mechanistic understanding of arrhythmogenesis in fibrotically remodelled hearts subjected to mechanical stress.

2. Methods

2.1 Cell culture model

Experiments were conducted in agreement with the relevant institutional and Swiss Federal guidelines for animal experimentation. Primary cultures of 1-day-old Wistar neonatal rat ventricular CMCs and MFBs were established using previously published methods.[12] Animals were decapitated, hearts removed, and the ventricular tissue was dissociated with trypsin. The resulting cell suspension containing CMCs and non-CMCs was subjected to differential pre-plating in order to separate fast adhering fibroblasts (dominating the cell type of non-CMC fraction) from slowly adhering CMCs. Adherent fibroblasts underwent a phenotype switch to MFBs within 1–2 days and were used in experiments after 8 days.

2.1.1 Single-cell cultures

For patch-clamp experiments, CMCs or MFBs were seeded at 40–500 cells/mm^2 on collagen- (Type I or IV, Sigma) coated glass coverslips or on silicone membranes. Before cell seeding, silicone membranes (Silastic, SMI, USA) were mounted on a digital caliper and pre-stretched by ~20%. A cell culture well was produced by glueing a silicone ring (28/2 mm; Semadeni, Switzerland) to the membrane with silicone adhesive. Experiments were performed on 3- to 4-day-old preparations.

2.1.2 Patterned growth cultures

For optical recording of impulse propagation under non-strained conditions, CMCs were seeded at a density of 1500 cells/mm^2 on photolithographically pretreated coverslips that were designed to produce uniform cell strands measuring 0.6 × 5 mm.[12] For strain experiments, lines of collagen were applied with a fine point nib (500–900 μm wide) to the bottom of the flexible culture wells. Hybrid CMC–MFB cell strands were obtained by coating 24-h-old CMC strand preparations with MFBs at a density of 500 cells/mm^2, which resulted in a CMC-to-MFB ratio of 3 : 1. Experiments were performed on 3- to 4-day-old preparations.

2.2 Optical measurement of impulse conduction

Impulse propagation along strand preparations was assessed optically using the voltage sensitive dye di-8-ANEPPS (Biotium). Experiments were conducted at 36°C and signals were recorded after pre-stimulation of the preparations for 10 s at 2 Hz. Recordings were made with a ×20 objective (spatial resolution: 50 μm). Signals acquired at 20 kHz were digitally filtered prior to analysis (f_c: 0.5 kHz). Optically recorded action potential amplitudes were normalized (%APA) and maximal upstroke velocities (dV/dt_{max}) were calculated in units of %APA/ms. For the case of an APA of 100 mV, values given in units of %APA/ms are identical to those in units of V/s.

2.3 Patch-clamp recording

Cell electrophysiology of CMCs and MFBs was assessed using standard whole-cell patch-clamp techniques (HEKA EPC-10). Signals were filtered (1 kHz), digitized (2.9 kHz), and stored for off-line analysis. The pipette filling solution contained (in mmol/L): K-aspartate 120, NaCl 10, MgATP 3, $CaCl_2$ 1, EGTA 10, and HEPES 5 (pH 7.2). Pipette resistances ranged from 4 to 6 MΩ. Series resistance and, after rupturing of the patch, cell capacitance were compensated and voltage values were corrected for liquid junction potentials (−12.4 mV). *I–V* relationships of CMCs and MFBs were obtained with voltage ramp protocols. Whole-cell currents were normalized to cell capacitance and are reported as pA/pF. For stretch/relaxation experiments, recordings were obtained within 25 min after application of defined levels of strain.

2.4 Wrinkle experiments

Substrates for the wrinkle assay (Excellness, Switzerland) were coated with collagen type IV, sterilized with UV, and coated with MFBs at low density (100 cells/mm^2). During experiments, preparations were continuously superfused at 36°C with Hank's balanced salt solution (HBSS) containing 1% neonatal calf serum (NCS). Time lapse video recordings served to assess the changes of wrinkle patterns following drug addition. A custom-made software (MatLab; The MathWorks, Natick, MA, USA) was used to quantify the time course of the change in the wrinkle area during experiments.

2.5 Immunocytochemistry

The presence of MFBs was confirmed by staining the preparations for α-smooth muscle actin and counterstaining the nuclei with DAPI using standard protocols.

2.6 Solutions

In all experiments, preparations were superfused at 2–3 mL/min with HBSS containing 1% NCS and 10 mmol/L of HEPES (pH 7.40). For gadolinium (Gd^{3+}) experiments, a solution devoid of phosphate and bicarbonate was used that contained (in mmol/L): NaCl 140, KCl 5.4, $CaCl_2$ 1.8, $MgCl_2$ 1.2,

glucose 20, HEPES 5 (pH 7.40). Drugs used were obtained from Sigma, except thrombin (Biopur AG, Switzerland).

2.7 Statistical analysis

Values are given as mean ± SD in the text and in the bar graphs. The number of samples refer to independent experiments. Data were compared using the two-tailed Student's *t*-test (homoscedastic or heteroscedastic where appropriate), and differences between data sets were considered significant at $P < 0.05$.

A detailed description of the methods used can be found in Supplementary material online.

3. Results

3.1 Validation of the experimental model

The effects of stretch and relaxation on action potential propagation were investigated in tissue-engineered cell strands grown on silicone membranes that were fixed to the arms of a sliding digital caliper (*Figure 1A*). During experiments, the entire assembly was placed on the stage of an inverted microscope, the preparation was superfused at 36°C and cell strands under investigation were stimulated with an extracellular electrode (*Figure 1B*). A typical example of optically recorded action potential upstrokes during propagated activity along a non-strained CMC cell strand is shown in *Figure 1C*. Experimental preparations consisted either of CMCs (CMC cell strands exhibiting a low degree of 'contamination' with MFBs; *Figure 2Aa*) or of CMC cell strands uniformly coated with MFBs (CMC–MFB cell strands; *Figure 2Ab*). Important in the context of patch-clamp experiments, fibroblasts seeded on silicone membranes displayed a rapid phenotype switch to MFBs as shown by abundant expression of α-smooth muscle actin containing stress fibres after 2 days in culture (*Figure 2Ac*). As shown in *Figure 2B* in a time series of images recorded with a high resolution camera (2048 × 2048 pixels, Ximea), strand preparations retained their stretched morphology beyond the maximal duration of the experiments. Being initially stretched by 5.5%, the example shown relaxes only slightly by 0.3% during 31 min of maintained stretch. As summarized in *Figure 2C*, this behaviour was typical for all four types of preparations used in this study, i.e. preparations retained their stretched geometry during prolonged application of static stretch (CMC strands: 0.01 ± 0.31%, $n = 16$; CMC–MFB strands: −0.07 ± 0.29%, $n = 22$; single-cell CMC preparations: −0.21 ± 0.70%, $n = 21$; single-cell MFB preparations: 0.26 ± 0.80%, $n = 10$; no significant differences among different types of preparations). Optical determinations of the dependence of conduction velocity on strain in CMC and CMC–MFB strands consisted of initial control measurements followed by recordings during constant application of 5% relaxation or 5% stretch, respectively. This was followed by control recordings after returning to initial conditions. Preparations were included in the analysis only if measurements obtained after returning to initial lengths were not statistically different from initial control recordings.

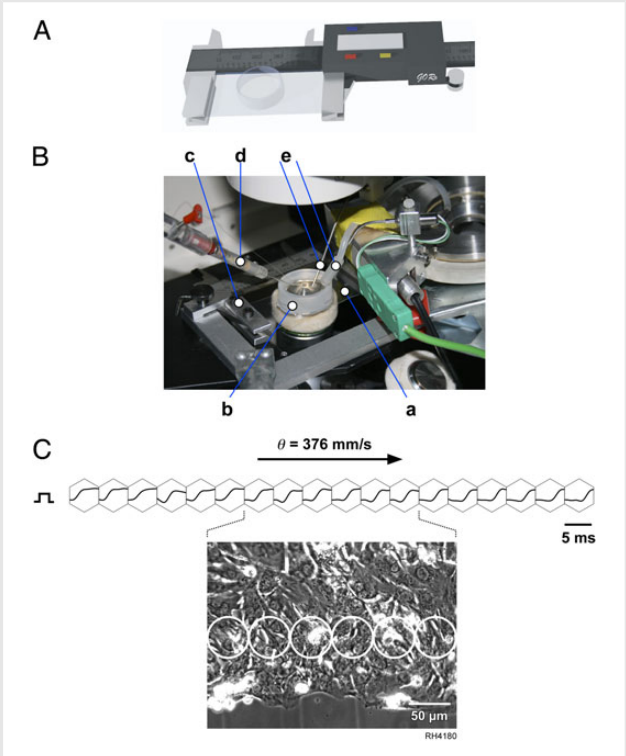

Figure 1 Experimental set-up. (*A*) Schematic drawing of the stretch device that consisted of a digital caliper whose jaws were attached to the culture 'dish' formed by a silicone ring glued to the rectangular silicone membrane. (*B*) Photograph of the stretch device mounted on the stage of an inverted microscope: (a) silicone membrane, (b) silicone ring, (c) left jaw of the caliper, (d) stimulation electrode, and (e) inlet/outlet of temperature-controlled superfusion system. (*C*) Example of an optical control measurement of a CMC strand preparation. Optical signals within hexagonal frames show action potential upstrokes of a propagated impulse measured by individual detectors. The morphology of the preparation is shown in the phase contrast image below with circles indicating the measurement areas of the central six photodetectors.

3.2 Effects of acute length changes on impulse conduction velocities and conduction times in cell strands

Conduction velocities in observer coordinates (θ_{observ}) were assessed at control lengths and immediately after stretching and relaxing the silicone membranes by 5% each (overall length change of 10.5%). As shown in *Figure 3A*, changing the overall length of CMC cell strands by 10.5% caused θ_{observ} to increase significantly by 7.1% from 325.7 ± 26.4 to 348.8 ± 39.9 mm/s ($n = 25$, $P < 0.05$). With 335.8 ± 27.8 mm/s, θ_{observ} recorded under non-strained control conditions fell exactly between θ_{observ} measured during relaxation and stretch, respectively. Maximal upstroke velocities (dV/dt_{max}) of propagating action potentials in CMC cell strands were not significantly affected by either manoeuvre (control: 71.4 ± 3.0%APA/ms; 5% stretch: 71.6 ± 5.0%APA/ms; 5% relaxation: 71.5 ± 4.0%APA/ms; $n = 25$, n.s.). A completely opposite behaviour was observed in CMC–MFB cell strands where changing the overall length by 10.5% caused θ_{observ} to decrease significantly by -12.5% from 291.4 ± 48.7 mm/s to 255.0 ± 46.6 mm/s (n=20, $P < 0.005$). With 276.7 ± 44.2 mm/s, θ_{observ} recorded under non-strained control conditions fell between θ_{observ} measured during relaxation and stretch, respectively. Maximal upstroke velocities were not significantly affected by the different strain conditions (control: 45.9 ± 13.4%APA/ms; 5% stretch: 45.6 ± 13.4%APA/ms; 5% relaxation: 47.6 ± 11.3%APA/ms; $n = 20$, n.s.).

Because preparations underwent defined levels of stretch and relaxation, changes of conduction times in preparation coordinates (CT_{prep})

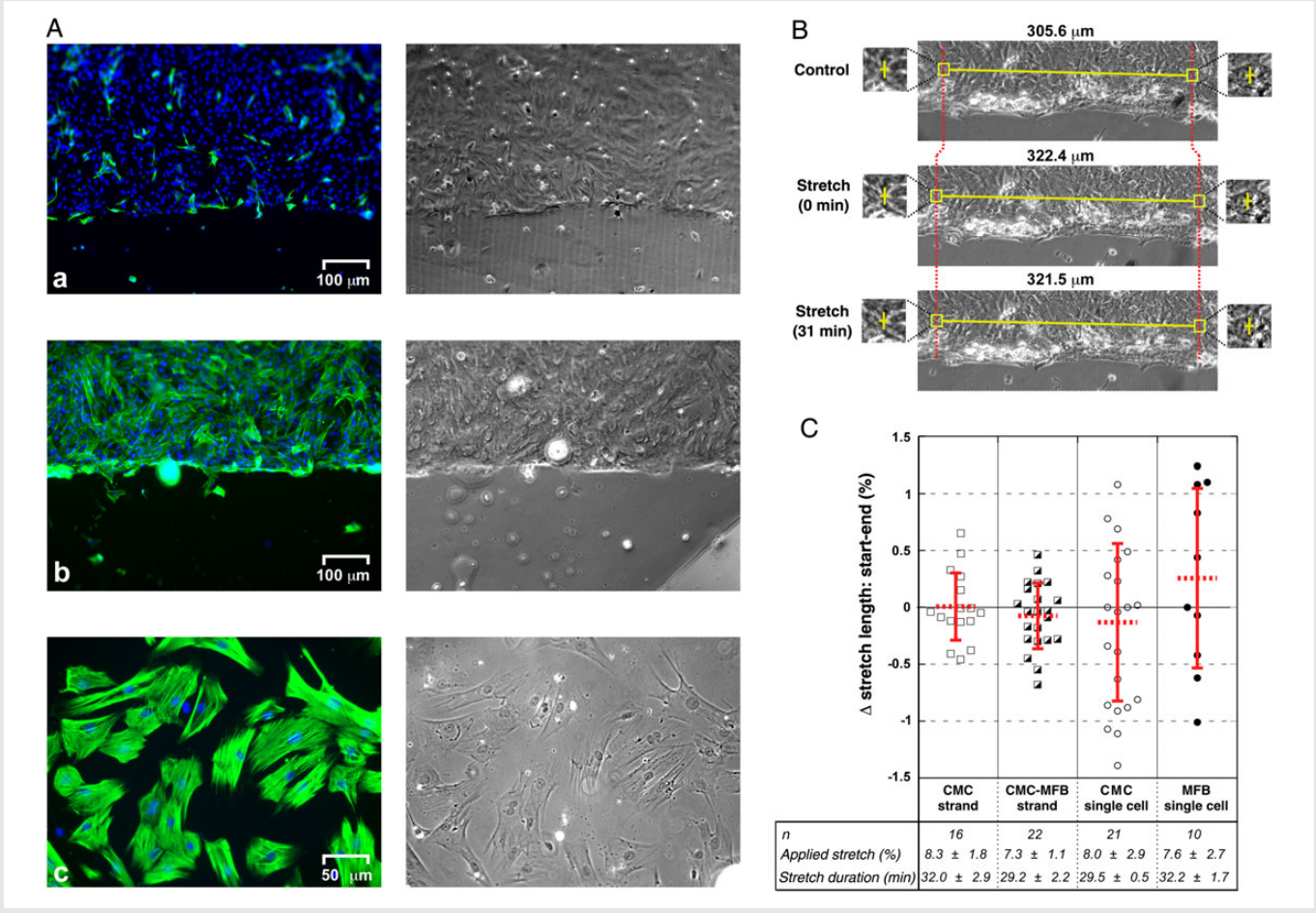

Figure 2 Structural characterization of preparations grown on silicone membranes and validation of the stretch procedure. (*A*) Structure and cellular composition of the experimental preparations: (*A*a) CMC cell strand with 'contaminating' MFBs [α-smooth muscle actin staining (green); nuclear counterstaining with DAPI (blue); corresponding phase contrast image on the right]. (*A*b) Same for a hybrid CMC–MFB cell strand. (*A*c) Same for single-cell MFB preparation as used in patch-clamp experiments. (*B*) Phase contrast images of the border region of a CMC strand before stretch (control), immediately after application of stretch, and at the end of a 31-min period of maintained stretch. Enlarged regions on both sides of the images depict the reference points within the preparation that were used for distance measurements. (*C*) Changes of the lengths of the four different types of experimental preparations (CMC cell strands, CMC–MFB cell strands, CMC single-cell cultures, and MFB single-cell cultures) along the main strain axis during stretch maintained for the duration and magnitude indicated.

during stretch and relaxation relative to control can be inferred by normalizing $\theta_{observ,\ intervention}$ to $\theta_{observ,\ control}$, followed by multiplication of the results with the length changes applied (0.95 for relaxation and 1.05 for stretch). The respective data shown in *Figure 3B* demonstrate that conduction times in CMC cell strands were not significantly affected by an overall lengthening of 10.5%. In contrast, the same amount of strain caused a highly significant increase of CT_{prep} in CMC–MFB cell strands (+26.3%; $P < 0.0001$).

3.3 Strain-induced mechanosensitive currents in MFBs and CMCs

To investigate whether modulation of conduction by strain is based on changes in resting polarization of CMCs and/or MFBs secondary to activation of MSCs, we assessed to which extent basic electrophysiological characteristics of the two cell types are affected by stretch. For this purpose, cells were grown at low densities on silicon membranes and were subjected to whole-cell patch-clamp recordings either under non-strained conditions or immediately after stretching the substrate by 5% (for detailed clamp protocols cf. Supplementary material online). In accordance with the protocols used for optical experiments, patch-clamp recordings were limited to 25 min following onset of static stretch. Mean *I–V* relationships obtained from MFBs under control conditions ($n = 13$) and during application of 5% stretch ($n = 8$) are shown in *Figure 4*Aa and b with *Figure 4*Ac, showing the superposition of the two *I–V* relationships. As can be gathered from the difference between the two relationships (*Figure 4*Ad), 5% stretch induced an outward rectifying current that reversed polarity at −12.8 mV. At −65 mV, a potential typically observed in CMC coupled to MFB,[13] stretch nearly doubled the inward current present under control conditions from -0.20 ± 0.11 to -0.36 ± 0.3 pA/pF. Neither cell capacitance (125.7 ± 67.9 vs. 125.3 ± 74.5 pF) nor input resistance (1.5 ± 0.6 vs. 1.1 ± 0.6 GΩ) of MFBs were significantly affected by stretch. The same type of experiments conducted with CMCs yielded, as illustrated by the stretch-induced difference current in *Figure 4*Bd (difference between the mean *I–V* relationships of 12 control and 13 stretched cells), a more complex response with no consistent stretch-induced changes at

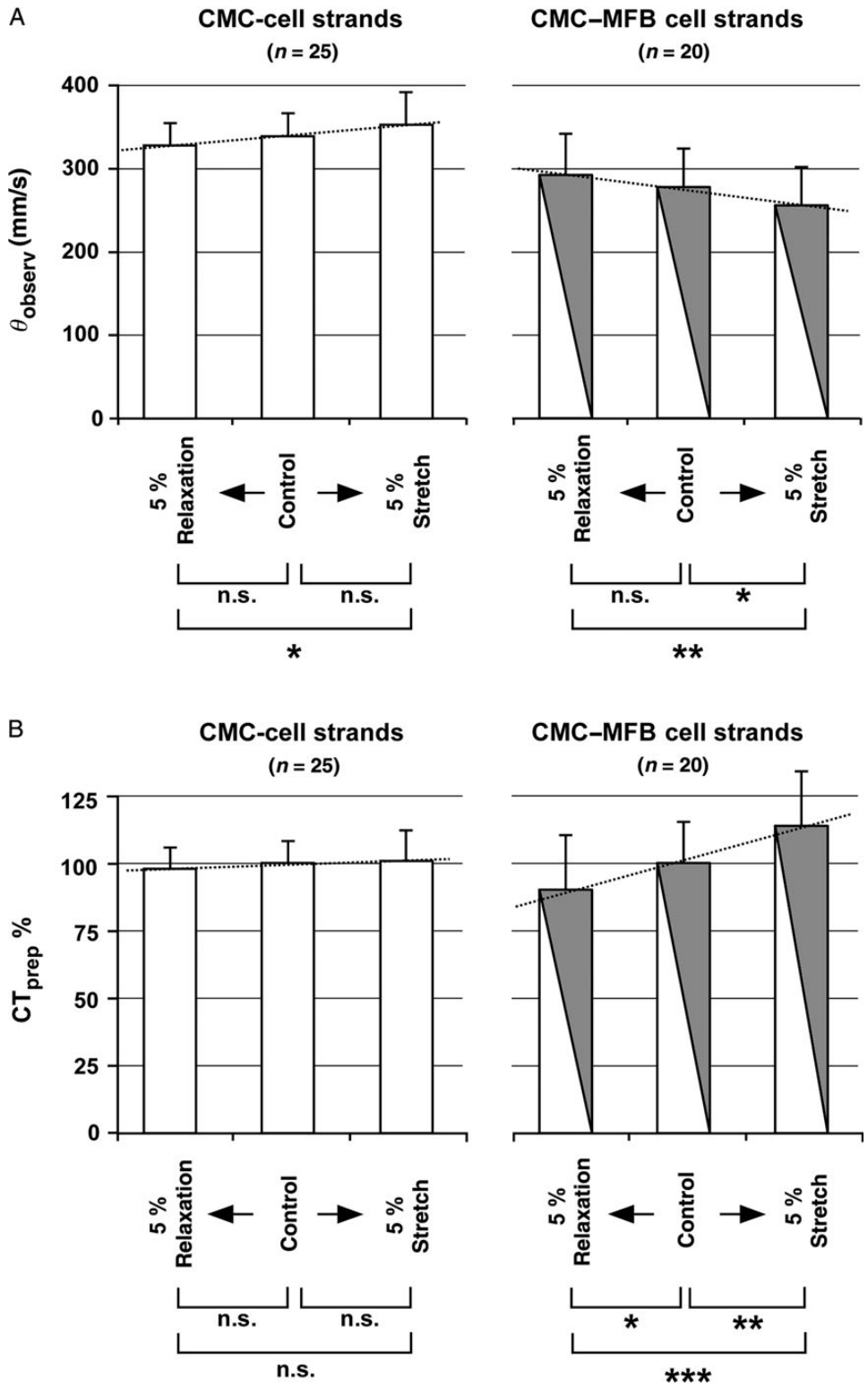

Figure 3 Effects of acute length changes of cell strands on conduction velocity and conduction times. (*A*) Impulse conduction velocity measured optically (θ_{observ}) along strands of CMCs (left panel) and hybrid CMC–MFB strands (right panel) during shortening ('relaxation') and extension ('stretch') of the preparations by 5% each. (*B*) Effects of stretch and relaxation on conduction times (CT_{prep}) of CMC cell strands (left panel) and hybrid CMC–MFB cell strands (right panel). Data are normalized to CT_{prep} obtained under control conditions. $^*P < 0.05$; $^{**}P < 0.005$; $^{***}P < 0.0005$.

potentials positive to −50 mV. Below this value, 5% stretch induced an inward current that reached a maximum at −76 mV (−0.2 pA/pF) before declining again and turning into an outward current at potentials negative to − 88 mV. Cell capacitance of CMCs was not significantly affected by stretch (18.4 ± 6.6 vs. 17.6 ± 9.6 pF), whereas their input resistance increased from 1.0 ± 0.5 to 2.4 ± 0.7 GΩ ($P < 0.005$). As

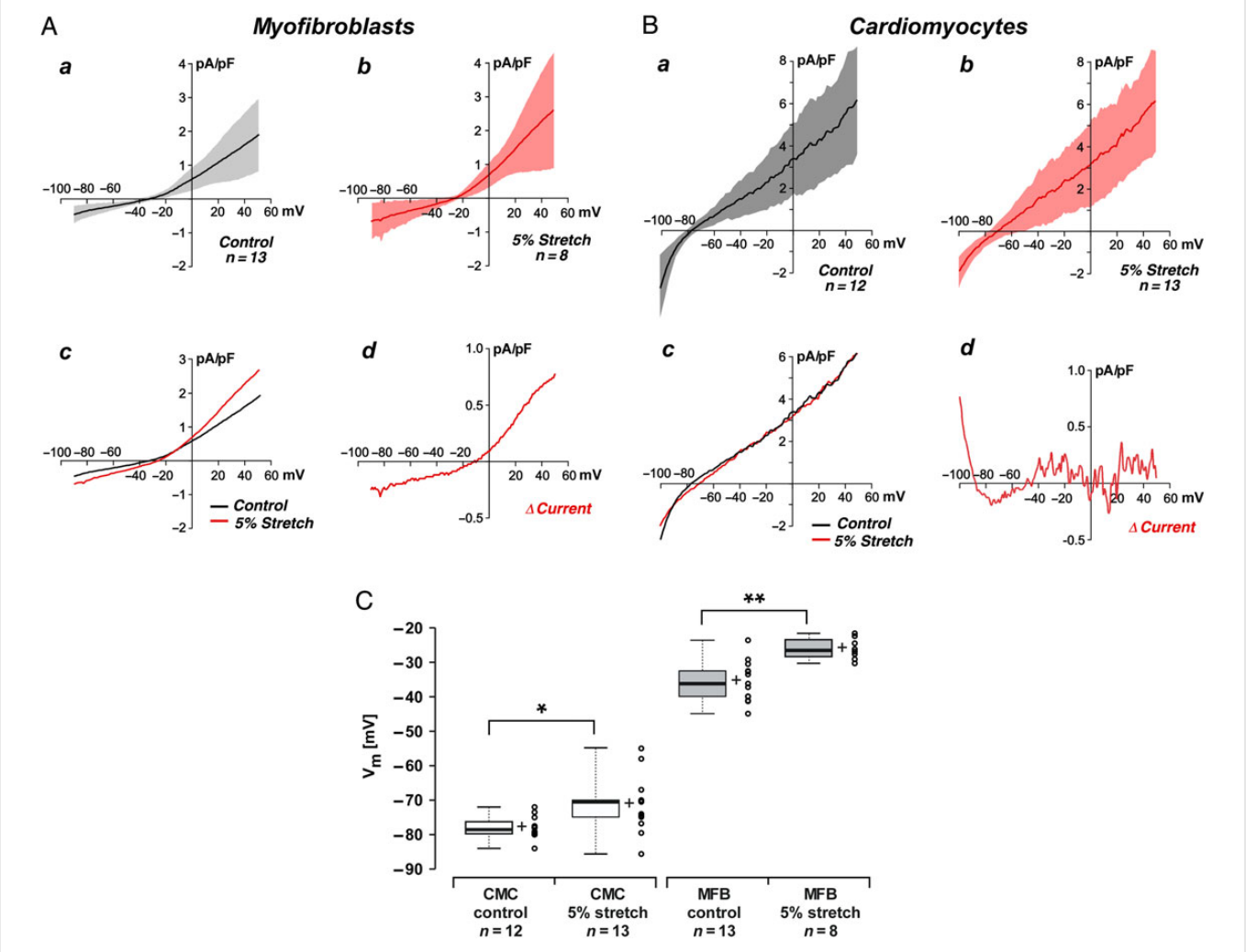

Figure 4 Effects of 5% stretch on single-cell electrophysiology of CMCs and MFBs. (*A*) Mean *I*–*V* relationships of MFBs obtained with ramp protocols under control conditions (*Aa*: mean ± SD; SD shown as band) and during application of 5% stretch (*Ab*). (*Ac*) Superposition of mean *I*–*V* curves obtained under control conditions (black) and during application of 5% stretch (red). (*Ad*) Mean difference current induced by 5% stretch. (*B*) Same as *A* for CMCs. (*C*) Change of membrane potential of CMCs and MFBs in response to application of 5% stretch. $^{*}P < 0.05$; $^{**}P < 0.005$.

shown in *Figure 4C*, strain-induced inward currents caused a significant reduction in the membrane potential of MFBs from −35.6 ± 5.9 (n = 13) to −26.1 ± 3.1 mV (n = 8; $P < 0.001$) and CMCs from −78.0 ± 3.2 (n = 12) to −70.8 ± 8.3 mV (n = 13; $P < 0.05$).

3.4 Contribution of MSCs to conduction under non-strained conditions

The finding that relaxation of CMC–MFB cell strands caused a significant decrease of conduction times suggested that MSCs of MFBs were contributing to conduction also under non-strained control conditions. Accordingly, we investigated the effects of the MSC blockers streptomycin (SM, 50 μmol/L) and Gd^{3+} (50 μmol/L; dissolved in appropriate low-phosphate buffers)[14] on the membrane voltage of CMCs and MFBs cultured under non-strained conditions. As shown in *Figure 5A*, the drugs had no effect on the resting polarization of CMCs (SM: −75.4 ± 1.3 vs. −75.7 ± 1.5 mV; n = 6, n.s.; Gd^{3+}: −76.1 ± 2.9 vs. −76.3 ± 2.9 mV; n = 11, n.s.), indicating that MSCs of CMCs were not active under non-strained conditions. In contrast, both MSC blockers caused MFBs to undergo a significant hyperpolarization (SM: −29.4 ± 7.8 to −34.3 ± 7.4 mV; n = 9, $P < 0.005$; Gd^{3+}: −32.2 ± 11.6 to −48.2 ± 11.7 mV; n = 9, $P < 0.005$), suggesting that MSCs contribute importantly to the membrane polarization of MFBs under non-strained conditions. In accordance with these single-cell data and as shown in *Figure 5B*, SM had no effect on θ (control: 336.3 ± 24.4 mm/s; SM: 329.5 ± 21.4 mm/s; n = 58; n.s.) and dV/dt_{max} (control: 75.2 ± 6.1%APA/ms; SM: 75.2 ± 5.3%APA/ms; n = 58; n.s.) in non-strained CMC cell strands. In contrast, SM caused a significant increase of both θ (173.8 ± 68.2 to 224.9 ± 63.3 mm/s; n = 54; $P < 0.005$) and dV/dt_{max} (29.8 ± 13.3 to 38.5 ± 14.3%APA/ms; n = 54; $P < 0.005$) in CMC–MFB cell strands. Because Gd^{3+} was substantially more effective in hyperpolarizing MFBs than SM, this compound was expected to surpass the effect of SM in increasing θ in CMC–MFB strands. However, both CMC and CMC–MFB strands consistently showed conduction blocks in the presence of Gd^{3+}, which is likely explained by its capacity to cause significant depression of sodium and calcium inward

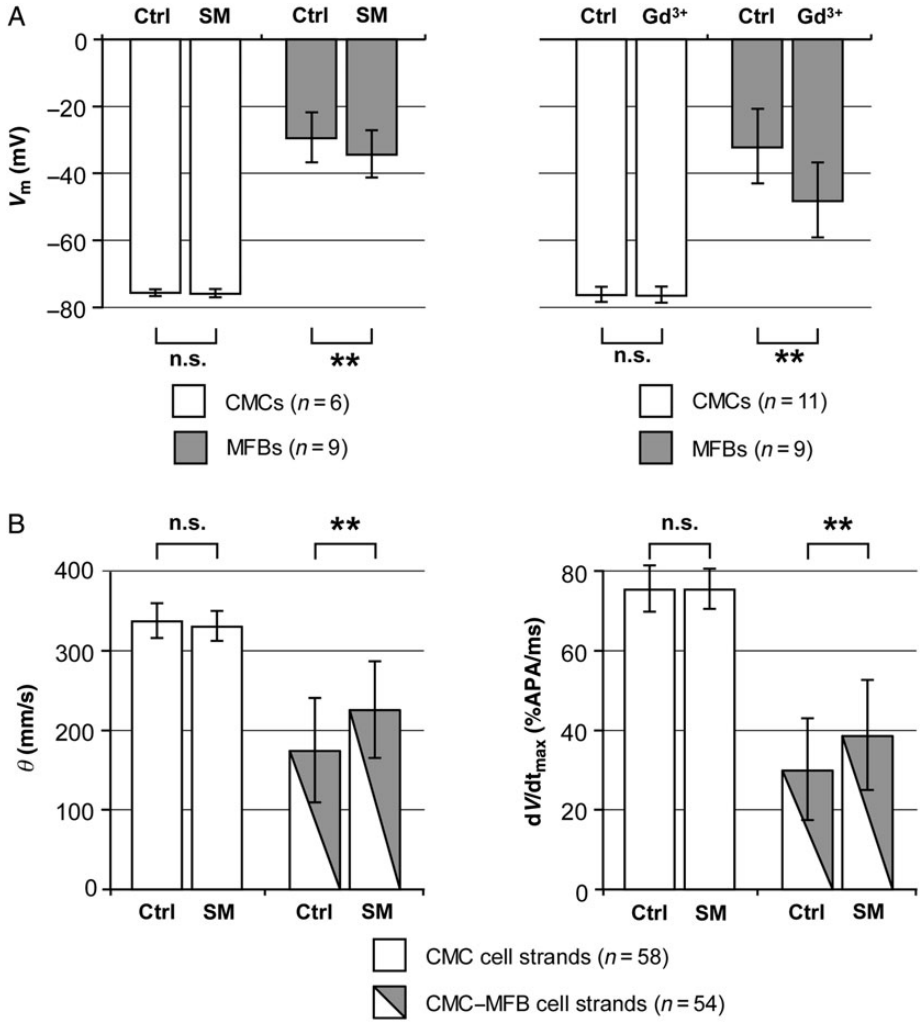

Figure 5 Effects of blocking MSCs on resting polarization and impulse propagation. (*A*) Change of resting polarization of CMCs and MFBs during exposure to SM (left panel) and Gd^{3+} (right panel). (*B*) Effect of SM on conduction velocity (θ; left panel) and maximal upstroke velocities (dV/dt_{max}; right panel) of propagated action potentials in CMC and CMC–MFB cell strands. $^{**}P < 0.005$.

currents in CMCs.[15,16] Overall, the results demonstrate that MFBs exhibit basal MSC activity under non-strained conditions that adds to their depolarized phenotype and, accordingly, contributes to slow conduction in CMC–MFB cell strands also under non-strained control conditions.

3.5 Effects of acute changes in the contractile state of MFBs on their membrane potential

Tension development is a characteristic feature of MFBs and, in the heart, is well established to be responsible for infarct scar consolidation.[17] The finding of basal MSC activity in non-strained MFBs raises the question of whether tension exerted by contractile MFBs on their substrate may feed back onto their own cell membrane in a manner that causes autoactivation of MSCs. This hypothesis was investigated by exposing MFBs to a blocker (blebbistatin) and an activator (thrombin) of MFB contractility.[18] The extent and time course of change of tension development by MFBs following addition of these drugs was assessed using a wrinkle assay, where the extent of deformation of the extracellular substrate (wrinkle formation) is a qualitative measure of tension exerted by adherent cells on the substrate.[19] In the example shown in *Figure 6A*, a single MFB caused extensive wrinkles in the substrate under control conditions. Following addition of 10 μmol/L blebbistatin to the superfusate, the area occupied by wrinkles declined by ∼50% within 10 min which reflects the drug-induced decrease of tension exerted by MFBs on their substrate (cf. also corresponding time lapse movie in Supplementary material online). Overall and as shown in *Figure 6B*, exposure of MFBs to 10 μmol/L of blebbistatin for 20 min caused a significant reduction in the wrinkle area by 30.3 ± 23.7% ($n = 9$, $P < 0.005$). Vice versa, exposure to 1 U/mL of thrombin caused the wrinkle area to increase by 75.2 ± 43.1% ($n = 10$; $P < 0.005$), which reflects a substantial increase of tension developed by MFBs. Time courses of the decrease (blebbistatin) and increase (thrombin) of the wrinkle area are shown in Supplementary material online, *Figure S1*. Determination of the resting polarization of MFBs exposed for a similar time to identical concentrations of the drugs demonstrated that blebbistatin had no significant effect on the membrane potential (control: −31.6 ± 11.2 mV;

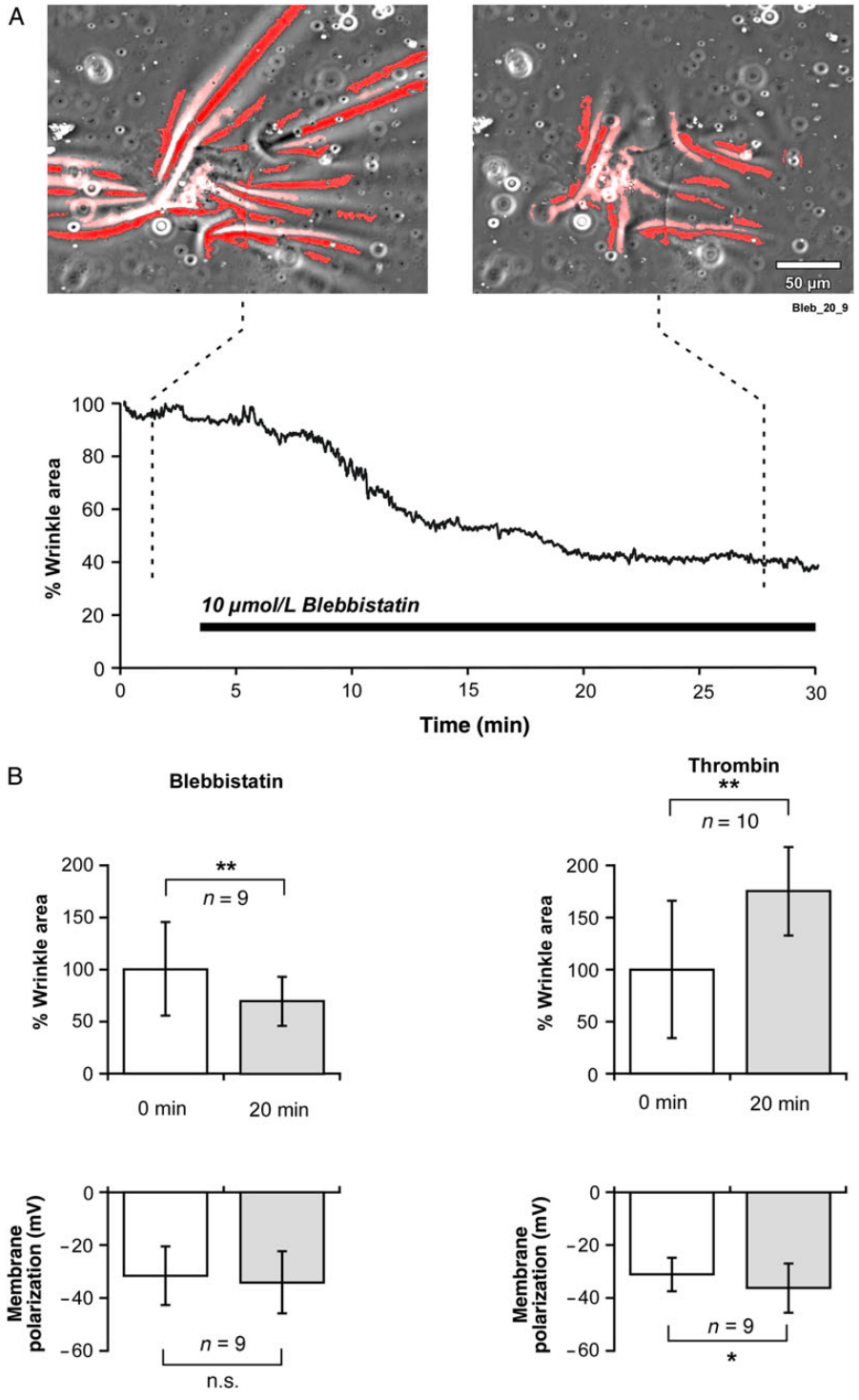

Figure 6 Modulation of MFB tension development by blebbistatin and thrombin. (*A*) Phase contrast images of wrinkle patterns before and after exposure of the preparation to blebbistatin (10 µmol/L). The panel below illustrates the time course of the reduction of the area occupied by wrinkles. (*B*) Effects of blebbistatin (left panels) and thrombin (right panels) on wrinkle formation and membrane potential of cardiac MFBs.

blebbistatin: -34.2 ± 11.8 mV; $n = 9$, n.s.), whereas thrombin, contrary to the hypothesis, caused a hyperpolarization despite increasing the tension developed by MFBs (control: 31.0 ± 6.4 mV; thrombin: -34.2 ± 9.2 mV; $n = 9, P < 0.05$). These findings suggest that MFB contractility does not directly contribute to basal activity of MSCs in non-strained preparations by auto-activation of these channels.

3.6 Effects of modulation of MFB contractility on impulse propagation in hybrid cell strands

For hybrid cell strands consisting of MFBs cultured on top of CMCs, mechanical tension developed by MFBs is likely to be transmitted by

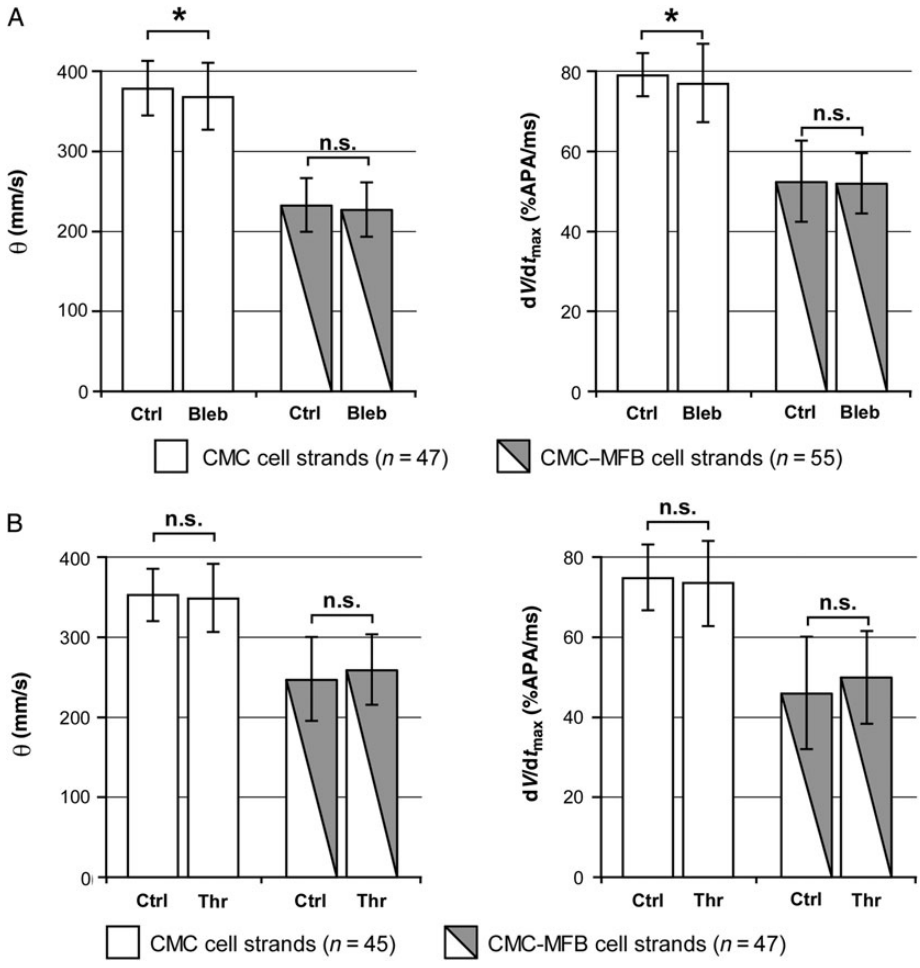

Figure 7 Effects of modulators of MFB contractility on impulse propagation in strand preparations. (*A*) Effects of reducing MFB contractility with blebbistatin on θ (left panel) and dV/dt_{max} (right panel) in CMC and CMC–MFB cell strands. (*B*) Effects of increasing MFB contractility with thrombin on θ (left panel) and dV/dt_{max} (right panel) in CMC and CMC–MFB cell strands.

adhesion junctions to underlying CMCs. Ensuing forces acting on the cell membrane of CMCs may modulate conduction by activation of MSCs in CMCs.[20] Accordingly, increasing (thrombin) or decreasing (blebbistatin) tension developed by MFBs attached to CMCs is expected to slow and accelerate conduction, respectively. As shown in *Figure 7A*, exposure of CMC cell strands to 10 μmol/L of blebbistatin for ≥20 min caused a slight reduction of θ from 375.7 ± 35.6 to 365.3 ± 42.9 mm/s ($n = 47$; $P < 0.05$) that was accompanied by an equally slight decrease of dV/dt_{max} from 78.8 ± 5.6 to 76.7 ± 10.1%APA/ms ($n = 47$; $P < 0.05$). In CMC–MFB cell strands, blebbistatin had no effects on θ (control: 230.6 ± 34.8 mm/s; blebbistatin: 225.2 ± 35.1 mm/s; $n = 55$; n.s.) and dV/dt_{max} (control: 52.2 ± 10.4%APA/ms; blebbistatin: 51.8 ± 7.8%APA/ms; $n = 55$; n.s.). As shown in *Figure 7B*, exposure of CMC cell strands to thrombin at 1 U/mL for ≥20 min had no effects on θ (control: 352.7 ± 34.2 mm/s; thrombin 348.2 ± 44.1 mm/s; $n = 45$; n.s.) and dV/dt_{max} (control: 74.8 ± 8.5%APA/ms; thrombin 73.4 ± 10.9%APA/ms; $n = 45$; n.s.). Similarly, in CMC–MFB strands, thrombin did neither affect θ (control: 246.6 ± 53.8 mm/s; thrombin 258.6 ± 45.9 mm/s; $n = 47$; n.s.) nor dV/dt_{max} (control: 45.8 ± 14.4%APA/ms; thrombin: 49.8 ± 11.9%APA/ms; $n = 47$; n.s.) The finding that neither blebbistatin nor thrombin affected conduction in hybrid cell strands suggests that tension exerted by MFBs on adjacent CMCs is not sufficient to modulate MSC activity of CMCs to an extent large enough to affect impulse conduction in hybrid CMC–MFB preparations.

4. Discussion

The results of this study demonstrate that impulse conduction in bioengineered strands of CMCs responds to moderate levels of relaxation and stretch highly similar to intact tissue, i.e. conduction times remain largely unchanged for physiological length changes as those encountered in end-diastole where maximal strain along the direction of the fibres amounts to ~10%.[11] In contrast, in the presence of MFBs simulating a fibrotically remodelled myocardium, impulse propagation is rendered highly sensitive to strain as reflected by a 3% increase of conduction time per each percent of lengthening. Given that the myocardium is maximally strained in end-diastole, these findings suggest that adverse electrotonic interactions between MFBs and CMCs are equally maximal at the time of electrical activation of the myocardium, thereby causing aggravation of slow conduction beyond values reported before for models of the fibrotically remodelled myocardium kept under isometric conditions.

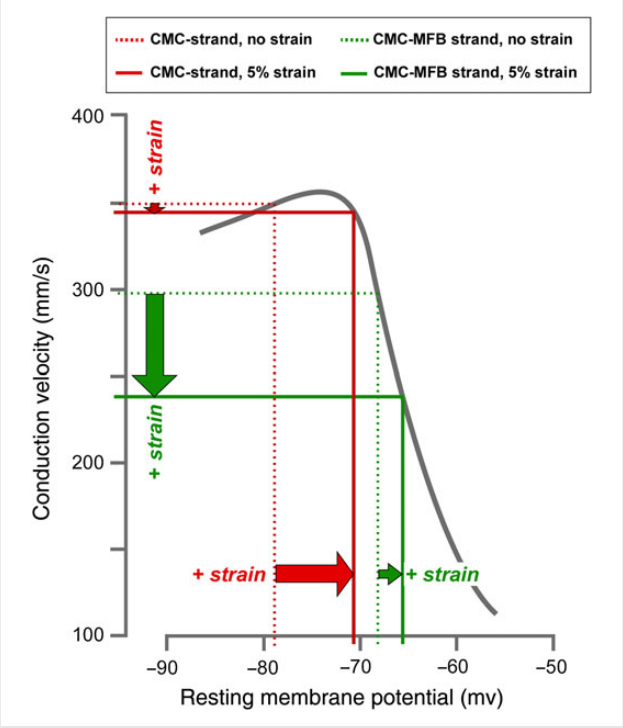

Figure 8 Schematic drawing illustrating the differential contributions of strain to conduction velocities in control CMC cell strands and in the fibrotic strand model consisting of CMC cell strands overlaid with MFBs. The grey curve indicates the dependence of θ measured in CMC cell strands on the resting membrane potential of CMCs ['supernormal conduction'; modified from ref. (27)]. The red lines refer to values obtained in CMC cell strands under non-strained control conditions (dashed) and during application of 5% strain (solid). A substantial stretch-induced depolarization of CMCs (horizontal red arrow) causes a modest change in conduction velocity (vertical red arrow). The green lines refer to values obtained in CMC–MFB cell strands (dashed = non-strained; solid = 5% strain). In these preparations, a modest stretch-induced depolarization (horizontal green arrow) causes a substantial change in conduction velocity (vertical green arrow).

4.1 Effects of strain on conduction in CMC preparations

Overall, elongation of CMC cell strands by 10.5% caused a significant increase of optically measured conduction velocities (θ_{observ}) from 326 to 349 mm/s (+7.1%). Under the simplifying assumption that electrical membrane properties and tissue resistance remained unaffected by the moderate amount of stretch applied, simple geometrical reasoning predicts that the increase of θ should equal the amount of stretch applied. θ_{observ} was slightly slower than this predicted value (7.1 vs. 10.5%) and, accordingly, CT_{prep} showed a small increase by 3.2%. In single CMCs, 5% strain induced a significant depolarization from −78 to −71 mV. This result is in agreement with previous studies using intact cardiac tissue or freshly isolated adult CMCs.[21,22] CMC depolarization was based on a strain-induced inward current that peaked at −76 mV, i.e. close to the resting potential of non-strained cells (−78 mV). The current declined in both the depolarizing and hyperpolarizing direction showing reversal potentials at −50 and −88 mV, respectively. While no further identification of this current was undertaken in the present study, a similar U-shaped mechanosensitive current observed in murine ventricular CMC was shown to be due to stretch-dependent inactivation of I_{K1}, which would explain the observation that strain significantly increased the input resistance of CMCs.[23,24] Assuming that CMCs forming the cell strands underwent the same degree of strain-induced depolarization, the finding that it had no major effect on θ is likely explained by the circumstance that conduction in cardiac tissue is little affected by changes in resting polarization in the range of −80 to −70 mV because of the presence of supernormal conduction.[25–27] This is illustrated schematically in *Figure 8*, where the grey curve depicts the dependence of conduction velocity on the resting membrane potential of CMCs as derived from a previous study with cultured strands of CMCs.[27] Typical for supernormal conduction, θ increases with increasing CMC depolarization from approximately −85 to −75 mV before declining rapidly with further depolarization. When inserting the resting potentials measured in this study for non-strained CMCs (approximately −78 mV) and CMCs subjected to 5% strain (approximately −71 mV) into this graph, it becomes evident that the substantial and significant depolarization of CMCs induced by 5% strain has a very limited effect on θ which is reflected by the experimental finding that conduction times remained unchanged during this intervention. Additional factors contributing to the modest dependence of θ on strain may include stretch-dependent modulation of sodium currents, membrane capacity, and intercellular resistance.[8,28–30] Important for this study, the results show that conduction in bioengineered strands of neonatal CMCs behaves identical to intact cardiac tissue from adult animals, i.e. conduction remains largely unchanged during application of physiological levels of strain which suggests that this preparation is a suitable model for investigating the effects of strain on conduction at the cellular level.[8,31,32]

4.2 Effect of strain on conduction in the fibrosis model

In contrast to the lack of significant effects of strain on conduction in CMC cell strands, applying identical strains to hybrid CMC–MFB cell strands caused a significant increase of conduction times by 26.3%. This contrasting result suggests that MFBs 'sensitize' CMCs to strain. The combination of three basic mechanisms as summarized schematically in *Figure 8* is likely to explain this observation: (i) as shown before, gap junctional coupling of moderately polarized MFBs to well-polarized CMCs causes convergence of the membrane potentials of the two cell types based on electronic current flow from MFBs to CMCs.[5] The resulting depolarization of CMCs to values less negative than −70 mV pushes non-strained networks of CMCs beyond membrane potentials supporting the peak of supernormal conduction, i.e. into a range where every additional depolarization further slows conduction due to increasing levels of sodium channel inactivation (*Figure 8*—green dashed lines).[25] (ii) As shown in this study, such additional depolarization is produced in CMCs by activation of MSC-dependent inward currents at potentials below −50 mV that aggravate the pre-existing, MFB induced depolarized state of CMCs. (iii) Additionally, strain applied to MFBs evokes mechanosensitive inward currents at potentials less negative than −12.8 mV. The resulting depolarization of MFBs will accentuate depolarizing current flow to electrotonically coupled CMCs, thereby further reducing the membrane voltage of CMCs (*Figure 8*—green solid lines). Overall, strain-induced activation of MSCs in both CMCs and MFBs that occur on top of the 'background' depolarization of CMCs by electrotonically coupled MFBs is likely to form the basis for the increased sensitivity of the fibrotic tissue model to strain. In

analogy, strain sensitivity of conduction may also be increased in other pathological conditions like hyperkalaemia or ischaemia where cardiac tissue is depolarized beyond membrane potentials supporting the peak of supernormal conduction.

4.3 Constitutive activity of MSCs in MFBs

The finding that relaxation of cell strands by 5% caused a significant decrease of conduction times in hybrid CMC–MFB cell strands, but not in CMC strands, suggests that the membrane polarization of MFBs but not CMCs is affected by basal activity of MSCs present under non-strained conditions. In accordance with previous findings in acutely isolated atrial fibroblasts,[9] the presence of constitutively active MSCs in MFBs but not CMCs was supported by the finding that two blockers of MSCs, SM and Gd^{3+}, caused a significant hyperpolarization of MFBs, but failed to affect the membrane voltage of CMCs under non-strained conditions. Consistent with the presence of basal activity of MSCs in MFBs that accentuates membrane depolarization of electrotonically coupled CMCs under non-strained conditions, superfusion of hybrid CMC–MFB cell strands with SM caused a significant increase of θ and dV/dt_{max}, but had no effect on CMC cell strands. While an even larger effect was expected to occur in the presence of Gd^{3+} that caused substantial hyperpolarization of MFBs, Gd^{3+} dissolved in the low-phosphate/low-bicarbonate superfusate necessary to prevent buffering of Gd^{3+} consistently induced conduction block.[14] Induction of block was likely related to the suppression of sodium and calcium inward currents by Gd^{3+}, which was reported to occur at concentrations similar to those used in the present study.[15,16] Overall, these findings suggest that the modest membrane polarization typically recorded from MFBs kept under non-strained conditions is partly due to depolarizing inward currents carried by constitutively active MSCs. Candidates for these MSCs include TRPC6, TRPM4, TRPM7, and TRPV2, which exhibit substantial expression at the mRNA level.[13] Immunocytochemistry revealed that TRPV2 is targeted to the cell membrane of MFBs at the site of the leading lamella, whereas TRPC6 shows increased expression at sites of cell-to-cell contact of neighbouring MFBs (cf. Supplementary material online).

4.4 Effect of MFB contractility on MSC activity and conduction in the fibrosis model

Given the presence of basal activity of MSCs in non-strained MFBs, the question arises as to whether this activity is due to tonic tensile forces exerted by MFBs that feed back onto their own cell membrane thereby causing 'auto-activation' of MSCs. This hypothesis was tested by assessing changes in membrane voltage of MFBs superfused with established activators (thrombin) and blockers (blebbistatin) of MFB contractility.[18] While, as shown by the wrinkle assay, both substances affected tension exerted by cardiac MFBs on their substrate according to expectations (increased tension with thrombin and reduced tension with blebbistatin), they did either not affect the membrane potential of MFBs (blebbistatin) or even caused a hyperpolarization (thrombin), which makes it unlikely that tension developed by MFBs causes auto-activation of MSCs.

Consistent with the small effects of blebbistatin and thrombin on the membrane potential of single MFBs, exposure of hybrid CMC–MFB cell strands to these drugs failed to affect θ and dV/dt_{max}. These findings demonstrate that modulation of MFB contractility alone is unable to affect impulse conduction in hybrid CMC–MFB preparations. This conclusion is supported by previous findings showing that communication incompetent HeLa cells, even though exerting tensile forces on their substrate similar to MFBs, fail to affect impulse propagation when seeded on top of CMC cell strands.[5,33]

5. Study limitations

In contrast to intact cardiac tissue undergoing phasic variations of strain, methodological restrictions imposed by the technique used in this study required measurements to be performed under static strain conditions. However, given that mechanosensitive currents of CMCs from rats and humans were reported before to activate promptly with applied strain and to display virtually no time dependence,[22] effects of phasic variations of strain on impulse conduction may be indirectly deduced from the strain—θ relationship presented in this study. Further limitations of the study are related to the question as to which extent the *in vitro* model reflects the situation *in vivo*: whereas the model used in this study is well characterized in terms of cellular morphology, heterocellular gap junctional coupling, ion current densities, and ratios of MFB-to-CMC cell membrane areas, the respective data from cells *in situ* are still largely missing because their measurement is technically not yet feasible. Accordingly, while the results contribute to the understanding of biophysical mechanisms governing conduction in strained cardiac tissue consisting of electrotonically interacting CMCs and MFBs, the extent to which these mechanisms are operational *in vivo* has to await the development of experimental methods suitable to investigate this question directly in intact tissue. This concerns especially the lack of unequivocal proof for the presence of heterocellular electrotonic coupling between MFBs and CMCs in the working myocardium of fibrotically remodelled hearts.[10,34] Also, it cannot be ruled out that fibroblasts present in intact hearts may add an additional layer of complexity to the response of cardiac tissue to stretch. Finally, the model used is based on neonatal rat ventricular cells. Whereas this limits extrapolations of results to intact human cardiac tissue, the finding that bioengineered preparations consisting predominantly of CMCs rather accurately reproduce the strain sensitivity of intact healthy tissue from adult mammals suggests that the biophysical principles governing the dependence of θ on strain are likely similar.

6. Conclusions

Whereas impulse conduction in healthy cardiac tissue shows little dependence on physiological levels of strain, the results of this study suggest that MFBs present in cardiac tissue undergoing fibrotic remodelling may convey increased strain sensitivity to the tissue with conduction velocities being inversely related to applied strain. Extrapolated to intact fibrotic tissue, this mechanism would imply that impulse conduction is slowest at the moment of electrical activation because activation coincides with the moment of maximal distension of the myocardium in end-diastole. Moreover, in diseased hearts displaying non-uniform mechanics, the mechanism may similarly increase non-uniformities of conduction. Pending verification in intact tissue, both effects would contribute to arrhythmogenesis in fibrotically remodelled myocardia.

Supplementary material

Supplementary material is available at *Cardiovascular Research* online.

Acknowledgements

We wish to thank Regula Flückiger-Labrada for her excellent cell culture work, Stephan Schmutz for the development of computer algorithms to quantify wrinkle formation, Jan Kucera for constructive discussions and for providing the theoretical basis for assessing substrate deformation, and Sarah Moyle for critically reading the manuscript.

Conflict of interest: none declared.

Funding

The work was supported by the Swiss National Science Foundation (138297 to S.R.), the European Network for Translational Research in AF (EUTRAF, 261057 to S.R.), and the Leducq Foundation (to S.R.).

References

1. Rohr S. Arrhythmogenic implications of fibroblast-myocyte interactions. *Circ Arrhythm Electrophysiol* 2012;**5**:442–452.
2. de Bakker JM, van Capelle FJ, Janse MJ, Tasseron S, Vermeulen JT, de Jonge N, Lahpor JR. Slow conduction in the infarcted human heart. 'Zigzag' course of activation. *Circulation* 1993;**88**:915–926.
3. Weber KT, Sun Y, Bhattacharya SK, Ahokas RA, Gerling IC. Myofibroblast-mediated mechanisms of pathological remodelling of the heart. *Nat Rev Cardiol* 2013;**10**:15–26.
4. Rohr S. Myofibroblasts in diseased hearts: new players in cardiac arrhythmias? *Heart Rhythm* 2009;**6**:848–856.
5. Miragoli M, Gaudesius G, Rohr S. Electrotonic modulation of cardiac impulse conduction by myofibroblasts. *Circ Res* 2006;**98**:801–810.
6. Miragoli M, Salvarani N, Rohr S. Myofibroblasts induce ectopic activity in cardiac tissue. *Circ Res* 2007;**101**:755–758.
7. Zlochiver S, Munoz V, Vikstrom KL, Taffet SM, Berenfeld O, Jalife J. Electrotonic myofibroblast-to-myocyte coupling increases propensity to reentrant arrhythmias in two-dimensional cardiac monolayers. *Biophys J* 2008;**95**:4469–4480.
8. McNary TG, Sohn K, Taccardi B, Sachse FB. Experimental and computational studies of strain-conduction velocity relationships in cardiac tissue. *Prog Biophys Mol Biol* 2008;**97**:383–400.
9. Kamkin A, Kiseleva I, Isenberg G. Activation and inactivation of a non-selective cation conductance by local mechanical deformation of acutely isolated cardiac fibroblasts. *Cardiovasc Res* 2003;**57**:793–803.
10. Kohl P, Kamkin AG, Kiseleva IS, Noble D. Mechanosensitive fibroblasts in the sino-atrial node region of rat heart: interaction with cardiomyocytes and possible role. *Exp Physiol* 1994;**79**:943–956.
11. Rademakers FE, Rogers WJ, Guier WH, Hutchins GM, Siu CO, Weisfeldt ML, Weiss JL, Shapiro EP. Relation of regional cross-fiber shortening to wall thickening in the intact heart. Three-dimensional strain analysis by NMR tagging. *Circulation* 1994;**89**:1174–1182.
12. Rohr S, Fluckiger-Labrada R, Kucera JP. Photolithographically defined deposition of attachment factors as a versatile method for patterning the growth of different cell types in culture. *Pflugers Arch* 2003;**446**:125–132.
13. Rosker C, Salvarani N, Schmutz S, Grand T, Rohr S. Abolishing myofibroblast arrhythmogeneicity by pharmacological ablation of alpha-smooth muscle actin containing stress fibers. *Circ Res* 2011;**109**:1120–1131.
14. Caldwell RA, Clemo HF, Baumgarten CM. Using gadolinium to identify stretch-activated channels: technical considerations. *Am J Physiol* 1998;**275**:C619–C621.
15. Lacampagne A, Gannier F, Argibay J, Garnier D, Le Guennec JY. The stretch-activated ion channel blocker gadolinium also blocks L-type calcium channels in isolated ventricular myocytes of the guinea-pig. *Biochim Biophys Acta* 1994;**1191**:205–208.
16. Li GR, Baumgarten CM. Modulation of cardiac Na^+ current by gadolinium, a blocker of stretch-induced arrhythmias. *Am J Physiol* 2001;**280**:H272–H279.
17. Sun Y, Weber KT. Infarct scar: a dynamic tissue. *Cardiovasc Res* 2000;**46**:250–256.
18. Wipff PJ, Rifkin DB, Meister JJ, Hinz B. Myofibroblast contraction activates latent TGF-beta1 from the extracellular matrix. *J Cell Biol* 2007;**179**:1311–1323.
19. Harris AK, Wild P, Stopak D. Silicone rubber substrata: a new wrinkle in the study of cell locomotion. *Science* 1980;**208**:177–179.
20. Thompson SA, Copeland CR, Reich DH, Tung L. Mechanical coupling between myofibroblasts and cardiomyocytes slows electric conduction in fibrotic cell monolayers. *Circulation* 2011;**123**:2083–2093.
21. Kamkin A, Kiseleva I, Wagner KD, Leiterer KP, Theres H, Scholz H, Gunther J, Lab MJ. Mechano-electric feedback in right atrium after left ventricular infarction in rats. *J Mol Cell Cardiol* 2000;**32**:465–477.
22. Kamkin A, Kiseleva I, Isenberg G. Stretch-activated currents in ventricular myocytes: amplitude and arrhythmogenic effects increase with hypertrophy. *Cardiovasc Res* 2000;**48**:409–420.
23. Dyachenko V, Husse B, Rueckschloss U, Isenberg G. Mechanical deformation of ventricular myocytes modulates both TRPC6 and Kir2.3 channels. *Cell Calcium* 2009;**45**:38–54.
24. McNary TG, Sachse FB. Modeling effects of strain-modulated membrane capacitance and conductance of k^+ inward rectifier on conduction velocity in cardiac tissue. *Cinc: 2009 36th Annual Computers in Cardiology Conference* 2009:381–384.
25. Kagiyama Y, Hill JL, Gettes LS. Interaction of acidosis and increased extracellular potassium on action potential characteristics and conduction in guinea pig ventricular muscle. *Circ Res* 1982;**51**:614–623.
26. Shaw RM, Rudy Y. Electrophysiologic effects of acute myocardial ischemia. A mechanistic investigation of action potential conduction and conduction failure. *Circ Res* 1997;**80**:124–138.
27. Rohr S, Kucera JP, Kleber AG. Slow conduction in cardiac tissue, I: effects of a reduction of excitability versus a reduction of electrical coupling on microconduction. *Circ Res* 1998;**83**:781–794.
28. Banderali U, Juranka PF, Clark RB, Giles WR, Morris CE. Impaired stretch modulation in potentially lethal cardiac sodium channel mutants. *Channels (Austin)* 2010;**4**:12–21.
29. Beyder A, Strege PR, Reyes S, Bernard CE, Terzic A, Makielski J, Ackerman MJ, Farrugia G. Ranolazine decreases mechanosensitivity of the voltage-gated sodium ion channel Na(v)1.5: a novel mechanism of drug action. *Circulation* 2012;**125**:2698–2706.
30. Mills RW, Narayan SM, McCulloch AD. Mechanisms of conduction slowing during myocardial stretch by ventricular volume loading in the rabbit. *Am J Physiol* 2008;**295**:H1270–H1278.
31. Penefsky ZJ, Hoffman BF. Effects of stretch on mechanical and electrical properties of cardiac muscle. *Am J Physiol* 1963;**204**:433–438.
32. Rosen MR, Legato MJ, Weiss RM. Developmental changes in impulse conduction in the canine heart. *Am J Physiol* 1981;**240**:H546–H554.
33. Wolfenson H, Bershadsky A, Henis YI, Geiger B. Actomyosin-generated tension controls the molecular kinetics of focal adhesions. *J Cell Sci* 2011;**124**:1425–1432.
34. Camelliti P, Green CR, LeGrice I, Kohl P. Fibroblast network in rabbit sinoatrial node: structural and functional identification of homogeneous and heterogeneous cell coupling. *Circ Res* 2004;**94**:828–835.